applied optics

Rainbows by elliptically deformed drops. I. Möbius shift for high-order rainbows

James A. Lock[1,*] and Gunther P. Können[2]

[1]Physics Department, Cleveland State University (retired), Cleveland, Ohio 44115, USA
[2]Royal Netherlands Meteorological Institute (retired), Sophialaan 4, NL-3761 DK Soest, The Netherlands
*Corresponding author: j.lock@csuohio.edu

Received 17 January 2017; accepted 22 March 2017; posted 19 April 2017 (Doc. ID 285001); published 15 May 2017

Using ray theory, the Möbius shift of the $(p-1)$-order rainbow angle for a particle having an elliptical cross section is obtained to first order in the ellipticity as a function of the tilt of the ellipse with respect to the propagation direction of the incoming rays. The result is then adapted to the geometry of scattering of light rays from the sun by a falling water drop as a function of sun height angle. The variation in the angular spacing between the supernumeraries is determined as a function of location along the rainbow arc, the conditions under which the rainbow angle is insensitive to drop flattening were determined, and the dependence of the Möbius shift on the drop refractive index is shown for rainbows up to fourth order $(p=5)$.

OCIS codes: (010.1290) Atmospheric optics; (080.0080) Geometric optics; (290.0290) Scattering; (290.1310) Atmospheric scattering.

https://doi.org/10.1364/AO.56.000G88

1. INTRODUCTION

Although credible reports of naked-eye observations of the third-order rainbow are rare due to its poor signal-to-background ratio [1], the visibility of naturally occurring high-order ($p\geq4$) rainbows has recently generated great interest due to the use of image processing techniques on photographs in which high-order rainbows were recorded but which were too dim to be discerned by the naked eye. In particular, image-processed photographic observations of the third-order [2], fourth-order [3], fifth-order [4], and possibly the seventh-order [5] natural rainbows have recently been published and analyzed [6]. The poor signal-to-background ratio of high-order rainbows has been compensated for in controlled laboratory experiments, where high-order rainbows [7–9] and rainbow glare spots [10] of a single pendant water droplet have been observed using a focused laser beam and a sensitive detector array. The incident laser beam is focused on the horizontal circular cross section of the pendant droplet near its edge, so that the ray path remains in the horizontal plane where the droplet cross section is circular. In addition, the focusing channels most of the laser power into rays in the vicinity of the Descartes ray. In the theoretical analysis of these laboratory experiments, the predicted rainbow deflection angle is obtained by adding the wave-theory-based Airy shift [11] to the ray-theory-based Descartes rainbow angle.

For natural rainbows, the shape of falling water drops is flattened by the combination of air resistance and surface tension forces [12–14]. Thus, light rays contributing to the top of the rainbow arc traverse the noncircular vertical cross section of the drop. The theoretical analysis of these observations of the natural rainbow includes an additional ray-theory-based shift of the rainbow angle, known as the Möbius shift. The shape of falling water drops whose volume-equivalent radius r is less than about 0.5 mm [12] can be accurately modeled by an oblate spheroid having a circular horizontal cross section and an elliptical vertical cross section. The shift of the rainbow deflection angle to first order in the ellipticity, called the first-order Möbius approximation to the ray theory Möbius shift, was determined for the first-order rainbow in [15,16] (see also [17]) and for the second-order rainbow in [18]. A short historical account of the modeling and observation of this shift before the time of Möbius is given in Appendix A. In spite of the large range of drop sizes in a typical rain shower, the supernumerary interference pattern accompanying the rainbow becomes observable when the opposing Airy and Möbius shifts produce a relative minimum of the supernumerary deflection angle as a function r, and there are plentiful drops in the rain shower of this size [17,18].

Light rays incident on a distorted water drop in other than the horizontal and vertical planes change their plane of propagation at every interaction with the drop surface. This causes their analysis to be considerably more complicated [19–21]. A simplifying approximation to the ray path inside the drop for a small deviation from sphericity is considered in Section 3.B. When the shape of a falling water drop can be accurately modeled by an oblate spheroid and a plane wave comprised of rays in all planes of incidence illuminates it in the side-on orientation, the first-order rainbow becomes part

of the more elaborate hyperbolic umbilic optical caustic [22–26]. As the water drop's deviation from circularity becomes more pronounced, the first-order rainbow scattering angle in the horizontal plane remains stationary while a transverse cusp caustic caused by the interference of skew rays slowly forms and moves toward it. Simultaneously, the first-order rainbow scattering angle in the vertical plane migrates toward the backscattering direction. This migration is the Möbius shift. This shift has been computed exactly in both wave theory [27] and ray theory [28] and has been compared with the first-order Möbius approximation [28,29].

In light of the recent interest in natural high-order rainbows, the purpose of this study is to determine the ray-theory-based first-order Möbius approximation for the general $(p-1)$-order rainbow for a water drop having an elliptical cross section in the vertical plane. A preliminary version of these results was reported previously [30] and was recently quoted in [28]. The validity of the first-order Möbius approximation depends on the interplay of two competing conditions. As a result, the falling water drops cannot be too small nor can they be too large. Specifically, the ray model of light scattering does not become quantitatively valid until the volume-equivalent radius r is much larger than the wavelength λ of the incident light. Experience has shown that $2\pi r/\lambda$ must be of the order of at least a few thousand [31–33]. For $\lambda = 0.55$ μm at the center of the visible spectrum, this criterion is roughly $r > 0.2$ mm. But as was mentioned above, the shape of a falling water drop is accurately modeled by an oblate spheroid for roughly $r < 0.5$ mm [12]. For radii larger than this, the bottom surface of the drop becomes increasingly flattened, and a two-ellipse cross section model of the shape in the vertical plane [34–36] provides a better approximation. Both ray theory and the spheroidal model of the falling water drop have been found to be valid for recent observations of the natural $(p-1)$-order rainbow. For example, in [17] the first two supernumeraries of the first-order rainbow were determined to be due to individual drops in the raindrop size distribution in the range $0.2\ \text{mm} \le r \le 0.3$ mm, and the drop sizes giving rise to the photographically observed high-order rainbows described in [4] were determined to be $0.26\ \text{mm} \le r \le 0.53$ mm.

The results of our study are presented in two papers: (i) the current Part I and (ii) Part II [37]. The body of the current paper is organized as follows. In Section 2, the first-order Möbius approximation to the ray-theory Möbius shift of the $(p-1)$-order rainbow is obtained for an elliptical cross section particle as a function of the orientation of the ellipse with respect to the direction of the incident rays. In Section 3, the ellipse orientation is referenced to the sun height angle in order to cast the result in terms of quantities standardly used in atmospheric observations, the formulas for the first-order and second-order rainbows are checked with those in earlier studies [18], and the formulas for high-order rainbows are given for tilted as well as for vertical scattering planes. For those who wish to have easy reference to the formulas for the first-order approximation to the Möbius shift for high-order rainbows in the vertical plane that were derived in detail in Sections 2 and 3, the appropriate formulas are tabulated in Appendix C. In Section 4, we study the dependence of the first-order Möbius approximation on the drop refractive index and determine the drop indices for which the first-order Möbius approximation vanishes, thus making the rainbow angle insensitive to drop flattening. In Section 5, we recount our major results and conclusions of this paper. Finally, in Part II of this study [37], the formulas of Airy theory are modified so as to include the Möbius shift, the variation of the angular spacing of the supernumeraries is determined as a function of the sun height angle, and conclusions about the appearance of supernumeraries of high-order rainbows in natural showers are drawn.

2. RAINBOWS FROM FLATTENED DROPS

A. Geometry of the Elliptical Cross Section

Consider the ellipse of Fig. 1 having its semi-major axis b along the y' axis and its semi-minor axis a along the x' axis:

$$x'^2/a^2 + y'^2/b^2 = 1. \tag{1}$$

For use in this Section, we define its ellipticity as

$$\epsilon \equiv (b/a) - 1, \tag{2}$$

and we consider the case where $b > a$ and $\epsilon > 0$. The ellipse and its $x'y'$ coordinate system are rotated by an angle ξ with respect to fixed x and y axes as in Fig. 2. A counterclockwise rotation is positive and a clockwise rotation is negative. We define the quantities A, E, and ζ describing the rotated ellipse by

$$A^2 \equiv b^2 \sin^2(\xi) + a^2 \cos^2(\xi), \tag{3a}$$

$$E \cos(\zeta) \equiv ab/A^2, \tag{3b}$$

$$E \sin(\zeta) \equiv (b^2 - a^2) \sin(\xi) \cos(\xi)/A^2, \tag{3c}$$

and we hereafter make use of the scaled coordinates

$$X \equiv x/A, \tag{4a}$$

$$Y \equiv y/A. \tag{4b}$$

The upper (+) and lower (−) surfaces of the rotated ellipse are given by

$$Y = -E \sin(\zeta) X \pm E \cos(\zeta)(1 - X^2)^{1/2}. \tag{5}$$

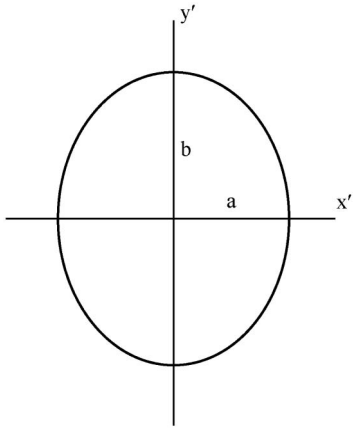

Fig. 1. Ellipse having semi-major axis b and semi-minor axis a. The coordinate frame of the ellipse is (x', y').

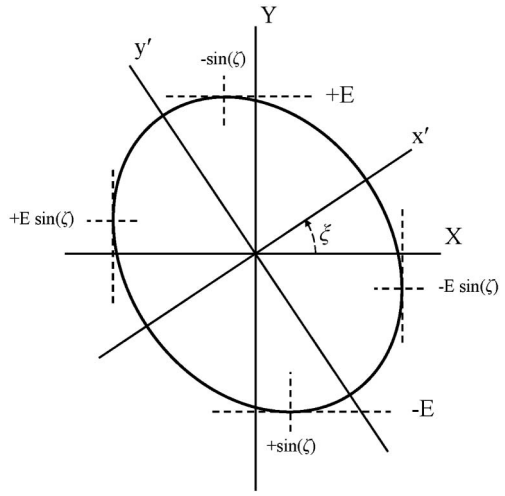

Fig. 2. Geometry of the ellipse of Fig. 1 whose frame (x', y') is rotated counterclockwise by the angle ξ with respect to frame (X, Y). See text for the meaning of the other symbols.

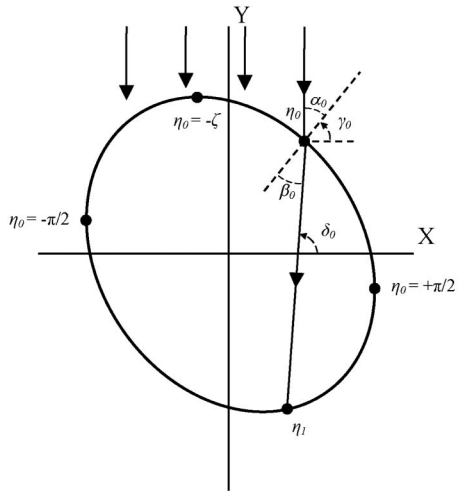

Fig. 3. Geometry of an incident ray refracted into the ellipse in the interval $-\zeta \le \eta_0 \le \pi/2$, in which η_0 is the point of incidence at the first interaction with the surface and η_1 is the point of incidence at the first internal reflection. The angle of incidence at the first interaction is α_0; its angle of refraction is β_0. See text for the meaning of the other symbols.

In order to clarify the physical meaning of A, E, and ζ, we note in Fig. 2 that (i) when $X = 0$, the Y axis intersects the top and bottom of the ellipse at $Y = \pm E\cos(\zeta)$, (ii) the lines tangent to the ellipse are vertical when $X = 1$, $Y = -E\sin(\zeta)$ and $X = -1$, $Y = E\sin(\zeta)$, (iii) the line tangent to the upper surface is horizontal when $X = -\sin(\zeta)$, $Y = E$, and the line tangent to the lower surface is horizontal when $X = \sin(\zeta)$, $Y = -E$. Thus, E and ζ describe both the degree of noncircularity of the ellipse and its clockwise or counterclockwise diagonal tilt. In the limit of a sphere, one has $b \to a$, $A \to a$, $E \to 1$, and $\zeta \to 0°$. Since $-1 \le X \le 1$ (or equivalently $-A \le x \le A$) on the ellipse perimeter, one can parameterize X by

$$X = \sin(\eta), \tag{6a}$$

where $-\pi/2 \le \eta \le \pi/2$ on the upper surface and $\pi/2 \le \eta \le 3\pi/2$ on the lower surface. Equation (5) then simplifies to

$$Y = E\sin(\eta + \zeta) \tag{6b}$$

on both the upper and lower surfaces of the ellipse.

B. Ray Propagation through the Rotated Ellipse

We consider a family of parallel light rays propagating vertically downward as in Fig. 3, which strike the upper surface of the ellipse. The first interaction of a ray with the surface is parameterized by the subscript 0. When the point of incidence of an incoming ray η_0 on the perimeter of the ellipse is in the range $-\pi/2 < \eta_0 < -\zeta$, the ray is refracted into the ellipse in the counterclockwise sense, and when $-\zeta < \eta_0 < \pi/2$, the ray is refracted in the clockwise sense. The angle γ_0 of the normal to the surface at the ray intersection point is measured counterclockwise with respect to the positive X axis.

From Eq. (5), one obtains

$$\gamma_0 = \arctan\{\cos(\eta_0)/[E\sin(\eta_0 + \zeta)]\}, \tag{7}$$

where the arctangent function is evaluated on its principal branch when $-\zeta < \eta_0 < \pi/2$, which is the situation considered here. The angle of incidence α_0 of the incoming ray is then

$$\alpha_0 = \pi/2 - \gamma_0, \tag{8}$$

and taking the interior of the ellipse to have the refractive index m, Snell's law gives the refracted angle β_0 as

$$\sin(\alpha_0) = m\sin(\beta_0). \tag{9}$$

The refracted ray makes an angle δ_0, measured counterclockwise from the positive X axis, giving

$$\delta_0 = \beta_0 + \gamma_0. \tag{10}$$

Using the equation for the slope of this line, the location η_1 where the refracted ray next strikes the ellipse on the lower surface is

$$\eta_1 = 2\arctan\{-[\tan(\delta_0) + E\sin(\zeta)]/[E\cos(\zeta)]\} - \eta_0 + 2N_1\pi, \tag{11}$$

where $N_1 = 1$ for $m = 1.333$, small ellipticity, and rays near the Descartes ray in the sphere limit. The precise meaning of the parameter N_1 that appears in Eq. (11) will be described in more detail following Eq. (16a). We are interested in ray paths in this angular region since the Möbius shift of the $(p-1)$-order rainbow for the elliptical cross section particle is determined here only for small ellipticity, where the path of the rainbow ray deviates to only $O(\epsilon)$ from the path of the Descartes ray for a circular cross section particle.

In order to trace the path of the ray from its $p-1$ interaction with the surface of the ellipse at η_{p-1} to its p interaction at η_p (where $p = 1$ for the initial interaction), one recursively follows the procedure of Eqs. (7)–(11), taking into account that the ray internally reflects at all interactions with the surface except for the last one, where it is refracted back out. For example, for the refracted ray of Eqs. (10) and (11) and in Fig. 4, the normal to the ellipse surface at the next interaction γ_1, given by

$$\gamma_1 = \arctan\{\cos(\eta_1)/[E\sin(\eta_1 + \zeta)]\} + M_1\pi, \tag{12}$$

is measured counterclockwise with respect to the positive X axis, where $M_1 = 1$ for $m = 1.333$, small ellipticity, and rays

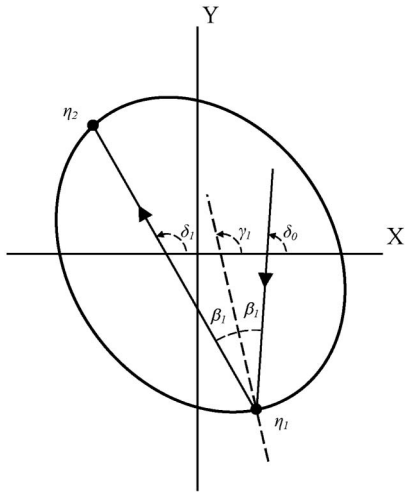

Fig. 4. Geometry of the first internal reflection of the ray of Fig. 3. See Fig. 3 for the meaning of the symbols.

near the Descartes ray in the sphere limit. The meaning of M_1 will be described in detail following Eq. (16b). The internal reflection angle β_1 is given by

$$\beta_1 = \gamma_1 - \delta_0, \tag{13}$$

and the angle the internally reflected ray makes with the positive X axis is δ_1, where

$$\delta_1 = 2\gamma_1 - \delta_0. \tag{14}$$

The internally reflected ray strikes the ellipse surface again at

$$\eta_2 = 2\arctan\{-[\tan(\delta_1) + E\sin(\zeta)]/[E\cos(\zeta)]\} - \eta_1 + 2N_2\pi, \tag{15}$$

where $N_2 = 2$ for $m = 1.333$, small ellipticity, and rays near the Descartes ray in the sphere limit.

In general, one has

$$\eta_{p+1} = 2\arctan\{-[\tan(\delta_p) + E\sin(\zeta)]/[E\cos(\zeta)]\} - \eta_p + 2N_{p+1}\pi \tag{16a}$$

for $1 \le p \le 7$, where $N_1 = 1, N_2 = N_3 = 2, N_4 = N_5 = 3$, and $N_6 = N_7 = N_8 = 4$ for $m = 1.333$, small ellipticity, and rays near the Descartes ray in the sphere limit. The meaning of N_{p+1} is as follows. From Eq. (6a), the angle that a line from the center of the ellipse to an internal reflection point at its surface makes with the positive vertical axis is η_p. As a ray makes an increasing number of internal reflections p, η_p increases as well. If the refractive index m is small, it takes more internal reflections for a ray to cycle once around beneath the ellipse surface, and if m is large, it takes fewer internal reflections for a ray to complete a cycle. So moving η_p to the left-hand side of Eq. (16a), the quantity $\eta_p + \eta_{p+1}$ continues to increase as the number of internal reflections increases. But the right-hand side of Eq. (16a) contains an arctangent function which is limited to the angular interval between $-\pi/2$ and $\pi/2$ on its principal branch. So as p increases, additional multiples of 2π, described by N_{p+1}, must be added to the arctangent to obtain $\eta_p + \eta_{p+1}$.

Another angle that describes the ray path and is of interest is

$$\gamma_p = \arctan\{\cos(\eta_p)/[E\sin(\eta_p + \zeta)]\} + M_p\pi, \tag{16b}$$

where $M_1 = M_2 = 1$, $M_3 = M_4 = 2$, $M_5 = M_6 = 3$, and $M_7 = M_8 = 4$ for $m = 1.333$, small ellipticity, and rays near the Descartes ray in the sphere limit. The interpretation of M_p is similar to that of N_p; the angle γ_p is geometrically constrained to be between 0 and π. But in the sphere limit, the arctangent function in Eq. (16b) reduces to $\pi/2 - \eta_p$. Again, since η_p continually increases as a function of p, a multiple of π, described by M_p, must be added to this in order to get into the range of γ_p. Since the number of internal reflections required for a ray to cycle around beneath the ellipse surface depends both on m and α_0, the quantities N_p and M_p depend on m and α_0 as well. Additional angles of interest are

$$\beta_p = \gamma_p - \delta_{p-1} + Q_p\pi, \tag{16c}$$

$$\delta_p = 2\gamma_p - \delta_{p-1} + Q_p\pi, \tag{16d}$$

with $Q_p = 1$ for $p = 2, 4, 6$, $Q_p = 0$ for $p = 1, 3, 5, 8$, and $Q_p = -1$ for $p = 7$.

The deflection angle Θ_p of the ray making $p - 1$ internal reflections before exiting the elliptical cross section particle, as measured clockwise with respect to the negative Y axis, is

$$\Theta_p = (\alpha_0 - \beta_0) + \sum_{q=1}^{p-1}(\pi - 2\beta_q) + (\alpha_p - \beta_p). \tag{17}$$

Thus far, the expressions for the ray path through the ellipse and the deflection angle have been exact. Since we are interested in the ray path inside an ellipse having a small ellipticity, we can expand the quantities E, ζ, γ_p, and η_{p+1} to first order in ϵ, giving

$$E = 1 + \epsilon\cos(2\xi) + O(\epsilon^2), \tag{18a}$$

$$\zeta = \epsilon\sin(2\xi) + O(\epsilon^2), \tag{18b}$$

$$\gamma_p = M_p\pi + \pi/2 - \eta_p - V_p\epsilon + O(\epsilon^2), \tag{18c}$$

$$\eta_{p+1} = 2\pi N_{p+1} - 2\delta_p - \eta_p + 2U_p\epsilon + O(\epsilon^2), \tag{18d}$$

where

$$U_p \equiv \cos(\delta_p)\sin(\delta_p - 2\xi), \tag{19a}$$

$$V_p \equiv \cos(\eta_p)\sin(\eta_p + 2\xi). \tag{19b}$$

It should be noted that the angles δ_p and η_p appearing in Eqs. (19a) and (19b) for U_p and V_p contain ϵ-dependence as well. But we will see shortly that the ϵ-dependence in these terms can be ignored if we are interested only in terms of $O(\epsilon)$ since U_p and V_p are already multiplied by ϵ in Eqs. (18c) and (18d).

It proves useful to express all the pertinent angles of the ray path, η_p, γ_p, β_p, α_p, and δ_p in terms of η_0, β_0 at the initial interaction, plus correction terms proportional to ϵ. We iterated

the procedure of Eqs. (16a)–(16d) for $1 \le p \le 8$ to $O(\epsilon)$ and found that

$$\eta_p = p\pi + \eta_0 - 2p\beta_0 + \epsilon\left[2pV_0 + \sum_{q=1}^{p-1}(4p-4q)V_q + \sum_{q=0}^{p-1}(4p-4q-2)U_q\right] + O(\epsilon^2), \tag{20a}$$

$$\gamma_p = (-R_p + 1/2)\pi - \eta_0 + 2\beta_0 - \epsilon\left[2pV_0 + \sum_{q=1}^{p-1}(4p-4q)V_q + V_p + \sum_{q=0}^{p-1}(4p-4q-2)U_q\right] + O(\epsilon^2), \tag{20b}$$

with $R_0 = R_1 = 0$, $R_2 = R_3 = 1$, $R_4 = R_5 = 2$, $R_6 = R_7 = 3$, and $R_8 = 4$ for $m = 1.333$ and rays near the Descartes ray in the sphere limit,

$$\beta_p = \beta_0 - \epsilon\left[V_0 + \sum_{q=1}^{p-1}2V_q + V_p + \sum_{q=0}^{p-1}2U_q\right] + O(\epsilon^2), \tag{20c}$$

$$\alpha_p = \alpha_0 - \epsilon[m\cos(\beta_0)/\cos(\alpha_0)] \times \left[V_0 + \sum_{q=1}^{p-1}2V_q + V_p + \sum_{q=0}^{p-1}2U_q\right] + O(\epsilon^2), \tag{20d}$$

$$\delta_p = (-S_p + 1/2)\pi - \eta_0 + (2p+1)\beta_0 - \epsilon\left[(2p+1)V_0 + \sum_{q=1}^{p}(4p-4q-2)V_q + \sum_{q=0}^{p-1}(4p-4q)U_q\right] + O(\epsilon^2), \tag{20e}$$

with $S_0 = S_1 = 0$, $S_2 = S_3 = 1$, $S_4 = S_5 = 2$, $S_6 = 3$, and $S_7 = S_8 = 4$ for $m = 1.333$ and rays near the Descartes ray in the sphere limit. Substituting Eq. (20c) for β_q for $1 \le q \le p$ and Eq. (20d) for α_p into Eq. (17), the deflection angle of a ray making $p-1$ internal reflections before exiting the elliptical cross section particle becomes

$$\Theta_p = (p-1)\pi + 2\alpha_0 - 2p\beta_0 + \epsilon T_p + O(\epsilon^2), \tag{21a}$$

where

$$T_p(\alpha_0) = (2p-1)V_0 + \sum_{q=1}^{p-1}(4p-4q)V_q + V_p + \sum_{q=0}^{p-1}(4p-4q-2)U_q - [m\cos(\beta_0)/\cos(\alpha_0)] \times \left[V_0 + \sum_{q=1}^{p-1}2V_q + V_p + \sum_{q=0}^{p-1}2U_q\right] + O(\epsilon^2). \tag{21b}$$

Recalling Eqs. (19a), (19b), (20a), and (20e), T_p can be thought of as a function of η_0, β_0, and α_0. But since η_0 can be expressed in terms of α_0, and β_0 is related to α_0 by Snell's law, it can be considered to be a function of α_0 alone. The condition

$$d\Theta_p/d\alpha_0 = 0 \tag{22}$$

for the occurrence of the $(p-1)$-order rainbow in ray theory for the elliptical cross section particle gives the value of α_0^R of the incident rainbow ray. The Taylor series expansion of α_0^R in powers of ϵ is of the general form

$$\alpha_0^R = \alpha_0^D + K\epsilon + O(\epsilon^2), \tag{23}$$

where the superscript R denotes the angle α_0 for the $(p-1)$-order rainbow ray of an elliptical cross section particle, the superscript D denotes α_0 for the $(p-1)$-order Descartes rainbow ray of a circular cross section particle, and K is a constant whose value is determined by the details of the derivatives in Eq. (22). Similarly, the Taylor series expansion of the refracted angle β_0^R in powers of ϵ is of the general form

$$\beta_0^R = \beta_0^D + C\epsilon + O(\epsilon^2), \tag{24}$$

where β_0^D is the refracted angle of the Descartes ray of a circular cross section particle and C is another constant. Snell's law relates the two constants by

$$C = K\cos(\alpha_0^D)/[m\cos(\beta_0^D)] + O(\epsilon). \tag{25}$$

The rainbow deflection angle is then

$$\Theta_p^R = \Theta_p^D + 2\epsilon(K - pC) + \epsilon T_p(\alpha_0^D + K\epsilon) + O(\epsilon^2). \tag{26}$$

Since we are interested in the Möbius shift of the $(p-1)$-order rainbow to only $O(\epsilon)$, two simplifications of Eq. (26) may be exploited. (i) The second term on the right-hand side of Eq. (26) vanishes to $O(\epsilon)$ independent of the value of the constant K since the angles of incidence and refraction of the Descartes ray for a sphere [i.e., $O(\epsilon^0)$] are related by

$$\cos(\beta_0^D) = (p/m)\cos(\alpha_0^D), \tag{27}$$

and (ii) since T_p in the third term on the right-hand side is already multiplied by ϵ, it can be evaluated at α_0^D in the sphere limit [i.e., again $O(\epsilon^0)$], bypassing the need to evaluate the constant K. One then has

$$\Theta_p^R = \Theta_p^D + \epsilon T_p(\alpha_0^D) + O(\epsilon^2). \tag{28}$$

The simplification of $T_p(\alpha_0^D)$ of Eq. (21b) is straightforward but lengthy and is summarized in Appendix B. We obtained

$$T_p = (-1)^{p+1}8\sin(\beta_0^D)\cos^3(\beta_0^D)F_p(2\beta_0^D)\cos(\Theta_p^D + 2\xi) + O(\epsilon^2) \tag{29}$$

for $2 \le p \le 9$. For even p, one has

$$F_2(2\beta_0^D) = 1, \tag{30a}$$

$$F_4(2\beta_0^D) = 12\cos^2(2\beta_0^D) - 2, \tag{30b}$$

$$F_6(2\beta_0^D) = 80\cos^4(2\beta_0^D) - 48\cos^2(2\beta_0^D) + 3, \tag{30c}$$

$$F_8(2\beta_0^D) = 448\cos^6(2\beta_0^D) - 480\cos^4(2\beta_0^D) + 120\cos^2(2\beta_0^D) - 4. \tag{30d}$$

For odd p, one has

$$F_3(2\beta_0^D) = 4\cos(2\beta_0^D), \tag{30e}$$

$$F_5(2\beta_0^D) = 32\cos^3(2\beta_0^D) - 12\cos(2\beta_0^D), \tag{30f}$$

$$F_7(2\beta_0^D) = 192\cos^5(2\beta_0^D) - 160\cos^3(2\beta_0^D) + 24\cos(2\beta_0^D), \tag{30g}$$

$$F_9(2\beta_0^D) = 1024\cos^7(2\beta_0^D) - 1344\cos^5(2\beta_0^D) + 480\cos^3(2\beta_0^D) - 40\cos(2\beta_0^D). \tag{30h}$$

As was done in [30], Eqs. (30a)–(30h) may be written as

$$F_{2M} = \sum_{m=0}^{M-1}(-1)^{M+m-1}[2\cos(2\beta_0^D)]^{2m} \times \{(M+m)!/[(M-m-1)!(2m)!]\}, \tag{31a}$$

$$F_{2M+1} = \sum_{m=0}^{M-1}(-1)^{M+m-1}[2\cos(2\beta_0^D)]^{2m+1} \times \{(M+m+1)!/[(M-m-1)!(2m+1)!]\}, \tag{31b}$$

where Eq. (31a) is used when p is even, and Eq. (31b) is used when p is odd. The coefficients of F_p in Eqs. (31a) and (31b) bear a similarity to the coefficients of Chebyshev polynomials of the second type [38]. Assuming this pattern continues for all $p \geq 10$, Eqs. (28), (29), (31a), and (31b) constitute the first-order Möbius approximation to the shift of angle of the $(p-1)$-order rainbow of a particle having an elliptical cross section.

3. PROPERTIES AND ZERO POINTS OF THE MÖBIUS FORMULA FOR OBLATE SPHEROIDS

A. Möbius Formula for the First-Order and Second-Order Rainbows

We next apply the results of Section 2 to an oblate spheroid with its symmetry axis vertical, which is the simplest approximation to the shape of falling drops of any liquid in still air [12,13]. To achieve this, we rotate the ellipse of Fig. 2 about the x' axis to generate an oblate spheroid whose three principal radii are $b \times b \times a$. As in Möbius' papers [15,16], we now parameterize the nonsphericity of the oblate spheroid by

$$\rho = [(b/a) - 1]/[(b/a) + 1]. \tag{32}$$

If b is only slightly larger than a, one has

$$\rho \approx \epsilon/2 + O(\epsilon^2). \tag{33}$$

However, in Section 2, the direction of the incoming rays was held fixed while the orientation of the ellipse was varied. For the remainder of this paper, the orientation of the falling oblate spheroidal droplet is held fixed while the direction of the incoming sunlight is varied. The direction of the incoming rays of sunlight with respect to the horizon is described by the sun height angle h as in Fig. 5. The conditions at sunrise or sunset when $h = 0°$ correspond in Figs. 2 and 3 to the semi-major axis being vertical (i.e., $\xi = 0°$).

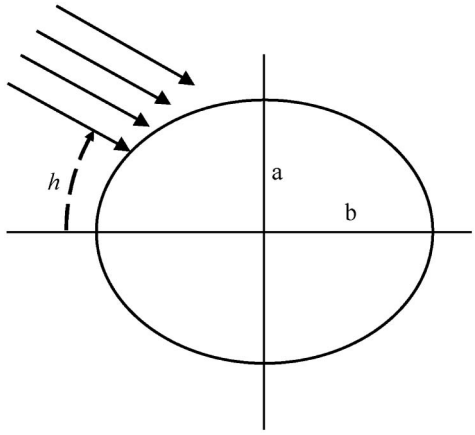

Fig. 5. Light rays from the sun with the sun height angle h incident on an oblate spheroidal falling water droplet.

First, as a check of the results for the first-order Möbius approximation given in Section 2, we consider the cases of the first-order and second-order rainbows for water drops. The top and bottom of the various order rainbows are defined as follows. Assume an observer is standing on a bridge just before sunset during a rain shower, so that $h \approx 0°$. The sun illuminates a large number of falling drops both above and below the observer's height and in both the direction toward the sun and away from it. Assume further that the observer sees a full 360° rainbow for each p. The incident light rays responsible for the top of the observed arc of the first-order rainbow strike drops above their horizontal centerline, with the drops being above the observer's height and opposite to the sun. As the sun's height angle increases, the location on the rainbow arc that was called the top for $h \approx 0°$ continues to be called the top. This situation corresponds to $\xi = h$ in Figs. 2 and 5. Equations (28), (29), and (30a) for $p = 2$ then become

$$\Theta_2^R = \Theta_2^D - 16\rho\sin(\beta_0^D)\cos^3(\beta_0^D)\cos(\Theta_2^D + 2h) + O(\rho^2), \tag{34}$$

in agreement with Eq. (3) of [18] as well as with Fraser's numerical ray-tracing experiments [17,39]. Incident light rays that are responsible for the bottom of the observed arc of the first-order rainbow when $h \approx 0°$ strike falling drops below their horizontal centerline, with the drops being below the observer's height and opposite to the sun. As h increases, this same location on the rainbow arc continues to be called the bottom of the rainbow. We give this precise definition of the "top" and "bottom" of the rainbow because the terms have not been applied uniformly in the literature, and because the transformation ξ into h for top and bottom is less trivial than it looks. For instance, the authors of [28] used a different convention, in which their "top" corresponds to our "bottom" and vice versa. As another example, Volz [40] in his discussion of the Möbius formula had applied the wrong sign in front of h [18].

In like manner, the incident light rays that are responsible for the top of the observed arc of the second-order rainbow when $h \approx 0°$ strike falling water drops below the droplet horizontal centerline, with the drops being above the observer's height and opposite to the sun. The incident light rays that

are responsible for the bottom of the observed arc of the second-order rainbow when $h \approx 0°$ strike the falling water droplets above the horizontal droplet centerline, with the drops being below the observer's height and opposite to the sun. This corresponds to $\xi = -h$ in Figs. 2 and 5. Equations (28), (29), and (30e) for $p = 3$ then become

$$\Theta_3^R = \Theta_3^D + 64\rho \sin(\beta_0^D)\cos^3(\beta_0^D)\cos(2\beta_0^D)\cos(\Theta_3^D - 2h) + O(\rho^2), \quad (35)$$

in agreement with Eq. (6) of [18].

B. Generalization to High-Order Rainbows and to Tilted Scattering Planes

Next we turn to the generic case and consider the ξ-dependent factor in the Möbius formula [Eq. (29)], which reads $\cos(\Theta_p^D + 2\xi)$. We first consider the top of the observed rainbow arc and with Fig. 5 we observe that (i) if the Descartes ray deflection angle Θ_p^D is in the second or first quadrant defined by the clockwise or counterclockwise progression of the ray path within the drop beginning from the forward scattering direction (e.g., the $p = 2$ and $p = 5$ bows for water), then $\xi = h$. Similarly, (ii) if Θ_p^D is the third or fourth quadrant defined by the progression of the ray path within the drop beginning from the forward scattering direction (e.g., the $p = 3$ and $p = 4$ bows for water), then $\xi = -h$. Then $\xi = h\,\mathrm{sgn}[\sin(\Theta_p^D)]$, where

$$\begin{aligned} \mathrm{sgn}(x) &= 1 \ \text{if}\ x > 0 \\ &= 0 \ \text{if}\ x = 0 \\ &= -1 \ \text{if}\ x < 0. \end{aligned} \quad (36)$$

Inserting this into $\cos(\Theta_p^D + 2\xi)$, one gets

$$\cos(\Theta_p^D + 2\xi) = \cos(\theta_p^D + 2h), \quad (37)$$

where $\theta_p^D \in [0, 180°]$ is the rainbow scattering angle, which is related to the rainbow deflection angle $\Theta_p^D \in [0, \infty)$ by

$$\theta_p^D = \arccos[\cos(\Theta_p^D)]. \quad (38)$$

Similarly, for the bottom of the observed rainbow arc one obtains

$$\cos(\Theta_p^D + 2\xi) = \cos(\theta_p^D - 2h), \quad (39)$$

which is valid for any Θ_p^D, p, and m. With these modifications and using Eq. (33) to relate ϵ and ρ, the generalized Möbius formula [Eq. (29)] for shift of the top and bottom of the observed rainbow arc generated by an oblate spheroid becomes

$$\Delta\Theta_p \equiv \Theta_p^R - \Theta_p^D = (-1)^{p+1}16\rho \sin(\beta_0^D)\cos^3(\beta_0^D)F_p(2\beta_0^D) \times \cos(\theta_p^D \pm 2h) + O(\rho^2), \quad (40)$$

in which the upper sign is for the top of the rainbow and the lower sign is for the bottom.

In the most general case, the scattering plane of an incident light ray is not vertical but is tilted from the vertical by the azimuthal angle φ. The intersection of the inclined scattering plane with a spheroid is again an ellipse. Assuming that the out-of-plane nature of the lightpath due to inclined refraction and reflection can be neglected to first order in ρ, one finds in accordance with Eq. (4) of Ref. [18] that

$$\Delta\Theta_p = (-1)^{p+1}16\rho' \sin(\beta_0^D)\cos^3(\beta_0^D)F_p(2\beta_0^D)\cos(\theta_p^D + 2h') + O(\rho^2), \quad (41a)$$

where

$$\rho' = \rho[1 - \sin^2(\varphi)\cos^2(h)] + O(\rho^2) \quad (41b)$$

is the effective value of the nonsphericity parameter of the droplet perimeter in the tilted scattering plane. In addition, h' is the angle between the major axis of the elliptical perimeter and the sun, where

$$\tan(h') = \tan(h)/\cos(\varphi). \quad (41c)$$

Equation (41a) reduces to Eq. (40) at the top of the rainbow where $\varphi = 0°$ and at the bottom of the rainbow where $\varphi = 180°$. The φ-dependence of the Möbius shift is evident for $h = 0°$, also known as side-on incidence, and unpolarized incident light in the wave scattering results of Figs. 5(b) and 5(c) of [27].

4. CONDITIONS FOR THE RAINBOW ANGLE TO BE INSENSITIVE TO THE NONSPHERICITY OF DROPS

In this section, the terms in Eq. (40) of order ρ^2 and higher are neglected for $\varphi = 0°, 180°$. In this case, we observe that $\Delta\Theta_p$ is zero if and only if one of the two last factors of Eq. (40) is zero:

$$F_p(2\beta_0^D)\cos(\theta_p^D \pm 2h) = 0. \quad (42)$$

We note from Eqs. (30a)–(30h) that $F_p(2\beta_0^D)$ is a function of $\cos(2\beta_0^D)$. Thus, for this analysis we split F into two factors S and P as

$$F_p(2\beta_0^D) = S_p[\cos(2\beta_0^D)]P_p[\cos^2(2\beta_0^D)], \quad (43)$$

in which

$$\begin{aligned} S_p[\cos(2\beta_0^D)] &= 1 \quad \text{for} \quad \text{even}\ p \\ &= \cos(2\beta_0^D) \quad \text{for} \quad \text{odd}\ p. \end{aligned} \quad (44)$$

The remaining factor $P_p[\cos^2(2\beta_0^D)]$ is a polynomial function of $\cos^2(2\beta_0^D)$ of degree 0 for $p = 2, 3$; of degree 1 for $p = 4, 5$; and so on. See Eqs. (30a)–(30h).

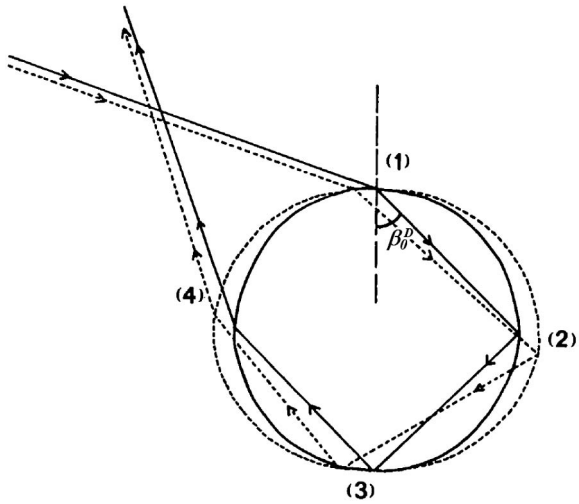

Fig. 6. For p = odd and rainbow angle of refraction $\beta_0^D = 45°$, the effect of drop flattening on the first $(p+1)/2$ interactions of the ray with the drop surface is to first order cancelled by the effect of drop flattening on the remaining $(p+1)/2$ interactions. This is illustrated here for $p = 3$ (the second-order rainbow).

Table 1. Möbius-Insensitive Indices of Refraction m for $h = 0°$ (Sun at the Horizon) and $1 < m < 2$

Rainbow Order	m	Factor that is Zero[a]	$\text{sign}(\partial\Delta\Theta_p/\partial m)$	$\text{sign}(\partial\Delta\Theta_p/\partial h)$[b]	Rainbow Deflection Angle	Rainbow Scattering Angle
First-order ($p = 2$)	1.1157	C	+	+	90.0°	90.0°
Second-order ($p = 3$)	1.0400	C	+	+	90.0°	90.0°
	1.3416	A	–	0	233.1°	126.9°
	1.1580	C	+	–	270.0°	90.0°
Third-order ($p = 4$)	1.0209	C	+	+	90.0°	90.0°
	1.1764	B	–	0	245.2°	114.8°
	1.2212	C	+	–	270.0°	90.0°
	1.7153	B	–	0	414.2°	54.2°
	1.9630	C	+	+	450.0°	90.0°
Fourth-order ($p = 5$)[c]	1.0130	C	+	+	90.0°	90.0°
	1.1084	B	–	0	250.0°	110.0°
	1.1285	C	+	–	270.0°	90.0°
	1.3868	A	–	0	427.4°	67.4°
	1.4451	C	+	+	450.0°	90.0°
Fifth-order ($p = 6$)[d]	1.0089	C	+	+	90.0°	90.0°
	1.0737	B	–	0	252.4°	107.6°
	1.0851	C	+	–	270.0°	90.0°
	1.2468	B	–	0	432.9°	72.9°
	1.2713	C	+	+	450.0°	90.0°
	1.6127	B	–	0	607.9°	112.1°
	1.6848	C	+	–	630.0°	90.0°

[a]Case A is $S_p[\cos(2\beta_0^D)] = 0$; Case B is $P_p[\cos^2(2\beta_0^D)] = 0$; Case C is $\cos(\theta_p^D) = 0$.
[b]Valid for the top of the rainbow.
[c]Two more zeros occur for $m = 2.1032$ (Case B) and $m = 2.4204$ (Case C), respectively.
[d]Two more zeros occur for $m = 2.4978$ (Case B) and $m = 2.8834$ (Case C), respectively.

The consequences of $S_p[\cos(2\beta_0^D)]=0$, or $P_p[\cos^2(2\beta_0^D)]=0$, or $\cos(\theta_p^D \pm 2h) = 0$ are as follows.

Case A: $S_p[\cos(2\beta_0^D)] = 0$. This occurs only for odd p and gives $\beta_0^D = 45°$. This implies that each two consecutive angles η where the Descartes ray hits the droplet surface are separated by 90°. If the number of interactions with the surface is even (hence p is odd), then for $\beta_0^D = 45°$ the effect of nonsphericity on the deviation of the ray in the first half of its path to $O(\rho)$ is counterbalanced by the effect in the second half of its path (see Fig. 6). For any odd p there is one value of m for which $\Delta\Theta_p(m)$ is zero due to $S_p[\cos(2\beta_0^D)] = 0$, independent of the value of the sun height angle h.

Case B: $P_p[\cos^2(2\beta_0^D)] = 0$. For $p > 3$ there are additional solutions for the increasingly more complicated rainbow ray paths, which result in insensitivity to droplet flattening. The polynomial character of P_p implies that there are two such additional flattening-neutral rainbow ray paths for $p = 4, 5$; four of them for $p = 6, 7$; and so on that are independent of h. We have not been able to find a simple geometrical interpretation of these additional neutral points.

Case C: $\cos(\theta_p^D \pm 2h) = 0$. If the bisector between the incoming rainbow ray and the emerging rainbow ray coincides with the major or minor axes of an ellipse, the lightpath inside the ellipse is symmetrical with respect to the axis. Then, the value of the shift $\Delta\Theta_p$ reaches an extremum: either a maximum (positive shift) or a minimum (negative shift). This situation occurs when $|\theta_p^D \pm 2h| = k\pi$. Between two consecutive extrema there should be a zero, corresponding to an inclined bisector with respect to the axis of the ellipse. Contrary to higher order Möbius approximations [37], in the first-order Möbius approximation considered here the oscillation term is a simple cosine function $\cos(\theta_p^D \pm 2h)$. This implies that for this approximation the zeros occur if $|\theta_p^D \pm 2h| = k\pi + \pi/2$, which corresponds to a situation where the bisector of the incoming and emerging rays coincides with a bisector of the two main axes of the ellipse. For a given value of h there are $p - 1$ values of m for which $\Delta\Theta_p(m) = 0$. If $h = 0°$ (sun at the horizon), this happens when the rainbow scattering angle θ_p^D is 90°.

Table 1 shows, for $1 < m < 2$ and $h = 0°$, the zero points of the Möbius shifts for rainbows up to order five ($2 \le p \le 6$) as well as the sign of $\partial\Theta_p/\partial m$ and $\partial\Theta_p/\partial h$. Figure 7 displays,

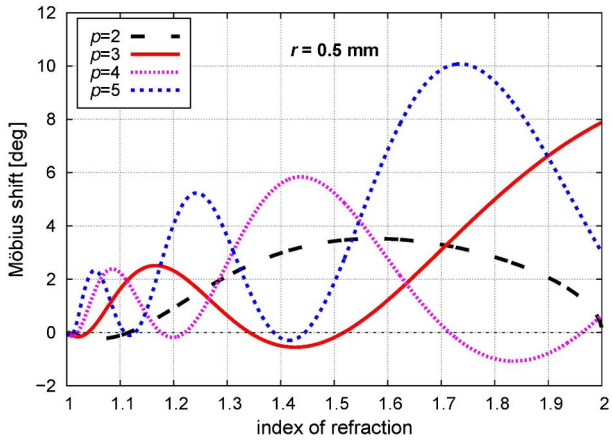

Fig. 7. Möbius shift as a function of index of refraction for the first-order ($p = 2$), second-order ($p = 3$), third-order ($p = 4$), and fourth-order ($p = 5$) rainbows for sun height 0°. Values are for $\rho = 0.025$, which corresponds to the ellipticity of falling water drops of radius 0.5 mm [13].

for $1 < m < 2$ and $h = 0°$, the Möbius shift for rainbows up to order 4 ($2 \le p \le 5$) for oblate spheroids with nonsphericity parameter $\rho = 0.025$.

5. DISCUSSION AND CONCLUSIONS

We have obtained a general formula for the Möbius shift of high-order rainbows to first order in the drop ellipticity. The extension of the first-order Möbius approximation to high-order ($p \ge 4$) rainbows is new, and their properties are explored by looking at the behavior of the shift as a function of m. It was found that the number of refractive indices at which the rainbow angle is insensitive to drop flattening increases with p. Some of these neutral points are independent of h. One cause of neutrality ($\beta_0^D = 45°$) occurs for odd values of p only. This geometry has been examined before for the second-order rainbow ($p = 3$) [18], but for larger values of p, other types of Descartes ray paths emerge for which the rainbow angle is insensitive to flattening. Their geometric significance is still to be unraveled.

When m turns out to be close to a neutral point, the first-order Möbius result is a poor approximation to the total Möbius shift. For water and visible light, this is only the case for the second-order rainbow ($p = 3$), and the Möbius term to second-order in ϵ or ρ must be invoked. For the $p \ne 3$ rainbows considered here, we believe that the first-order Möbius approximation gives sufficiently accurate results to be used for the present analysis of supernumeraries. This belief emerges from an evaluation of the $O(\rho^2)$ Möbius term for $p = 3$ [37], which suggests that for the other rainbows, the $O(\rho^2)$ Möbius term for $a \approx 0.5$ mm is a correction to the maximum rainbow shift of order ~1%. This accuracy is more than sufficient for our purpose. Further ray-tracing computations are needed to obtain an improved assessment of the accuracy of the first-order Möbius approximation.

APPENDIX A: HISTORICAL ASIDE

As an historical aside, in his 1961 paper in *Handbuch der Geophysik VIII* [40], F. E. Volz noted that in 1814 Venturi knew that the rainbow angle shifts with the flattening of the drops and had calculated the "Möbius shift" for $h = 0°$ using a simplified model for the shape of oblate raindrops. He successfully checked his model experimentally with a suitable optical setup [41]. For a given aspect ratio b/a, he thus obtained the "Venturi shift," which turns out to be about twice as large as the Möbius shift for a spheroidal drop. He then conjectured that rainbow supernumeraries were the result of the existence of two different droplet sizes in a rain shower. One population of droplets was small and spherical, producing the normal rainbow. The other population was large and flattened, giving rise to a shifted rainbow: the supernumerary. As we know now, this is not the mechanism that produces supernumeraries but instead generates twinned rainbows [35]. Venturi's paper was translated from Italian into German and commented on by H. W. Brandes in 1816 [42].

APPENDIX B: SIMPLIFICATION OF $T_p(\alpha_0^D)$ IN EQ. (28)

The simplification of $T_p(\alpha_0^D)$ in Eq. (28) to yield the result of Eqs. (29)–(31) is summarized as follows. (i) As was mentioned after Eq. (19b), one substitutes δ_q and η_q of Eqs. (20a) and (20e) to $O(\epsilon^0)$ into the expressions for U_q and V_q in Eqs. (19a) and (19b), respectively, in order to obtain these quantities to $O(\epsilon^0)$. (ii) One substitutes the resulting U_q and V_q into T_p of Eq. (21b) to obtain T_p to $O(\epsilon^0)$. (iii) One rearranges T_p so as to factor out $(-1)^{p+1}\cos(\Theta_p^D + 2\xi)$. The remaining portion of T_p can be written as

$$(p-1)\sin(p\chi) + \sum_{r=0}^{p-2} 2(p-1-r)\sin[(p-1-r)\chi], \tag{B1}$$

where

$$\chi = 2\beta_0^D. \tag{B2}$$

(iv) One then writes $\sin[(p-1-r)\chi]$ in terms of powers of $\cos(\chi)$ and $\sin(\chi)$ and factors out

$$2\sin(\chi)[1+\cos(\chi)] = 8\sin(\beta_0^D)\cos^3(\beta_0^D) \tag{B3}$$

from Expression (B1). The remaining portion is $F_p(\chi)$ of Eqs. (30a)–(30h) and (31a) and (31b).

APPENDIX C: EXPLICIT MÖBIUS FORMULA FOR RAINBOWS UP TO ORDER FIVE ($p = 6$)

The deflection angle and scattering angle of the $(p-1)$-order rainbow are Θ_p^R and θ_p^R, respectively; the Möbius shift of the deflection angle is $\Delta\Theta_p \equiv \Theta_p^R - \Theta_p^D$; the angle of refraction of the Descartes ray, β_0^D, for the $(p-1)$-order rainbow for a spherical particle used in the body of this paper is here denoted by β_p; $\rho \equiv (b-a)/(b+a)$ parameterizes the nonsphericity of the oblate spheroid; h is the sun height angle. All formulas refer to the top of the rainbows; for their bottoms, the plus sign in front of h should be replaced by a minus sign. We have

$$\Delta\Theta_2 = -16\rho\sin(\beta_2)\cos^3(\beta_2)\cos(\theta_2 + 2h) + O(\rho^2), \tag{C1}$$

$$\Delta\Theta_3 = +64\rho\sin(\beta_3)\cos^3(\beta_3)\cos(2\beta_3)\cos(\theta_3 + 2h) + O(\rho^2), \tag{C2}$$

$$\Delta\Theta_4 = -32\rho\sin(\beta_4)\cos^3(\beta_4)[6\cos^2(2\beta_4) - 1]\cos(\theta_4 + 2h) + O(\rho^2), \tag{C3}$$

$$\Delta\Theta_5 = +64\rho\sin(\beta_5)\cos^3(\beta_5)\cos(2\beta_5)[8\cos^2(2\beta_5) - 3] \times \cos(\theta_5 + 2h) + O(\rho^2), \tag{C4}$$

$$\Delta\Theta_6 = -48\rho\sin(\beta_6)\cos^3(\beta_6)\left[\frac{80}{3}\cos^4(2\beta_6) - 16\cos^2(2\beta_6) + 1\right] \times \cos(\theta_6 + 2h) + O(\rho^2). \tag{C5}$$

REFERENCES AND NOTES

1. R. L. Lee and P. Laven, "Visibility of natural tertiary rainbows," Appl. Opt. **50**, F152–F161 (2011).
2. M. Großmann, E. Schmidt, and A. Haußmann, "Photographic evidence for the third-order rainbow," Appl. Opt. **50**, F134–F141 (2011).
3. M. Theusner, "Photographic observation of a natural fourth-order rainbow," Appl. Opt. **50**, F129–F133 (2011).

4. H. E. Edens, "Photographic observation of a natural fifth-order rainbow," Appl. Opt. **54**, B26–B34 (2015).
5. H. E. Edens and G. P. Können, "Probable photographic detection of the natural seventh-order rainbow," Appl. Opt. **54**, B93–B96 (2015).
6. G. P. Können, "Polarization and visibility of higher-order rainbows," Appl. Opt. **54**, B35–B40 (2015).
7. K. Sassen, "Angular scattering and rainbow formation in pendant drops," J. Opt. Soc. Am. **69**, 1083–1089 (1979).
8. C. W. Chan and W. K. Lee, "Measurement of liquid refractive index by using high-order rainbows," J. Opt. Soc. Am. B **13**, 532–535 (1996).
9. P. H. Ng, M. Y. Tse, and W. K. Lee, "Observation of high-order rainbows formed by a pendant drop," J. Opt. Soc. Am. B **15**, 2782–2787 (1998).
10. J. D. Walker, "Multiple rainbows from single drops of water and other liquids," Am. J. Phys. **44**, 421–433 (1976).
11. H. C. van de Hulst, *Light Scattering by Small Particles* (Dover, 1981), pp. 243–246.
12. H. R. Pruppacher and R. L. Pitter, "A semi-empirical determination of the shape of cloud and rain drops," J. Atm. Sci. **28**, 86–94 (1971).
13. A. W. Green, "An approximation for the shapes of large raindrops," J. Appl. Meteorol. **14**, 1578–1583 (1975).
14. K. V. Beard and C. Chuang, "A new model for the equilibrium shape of raindrops," J. Atm. Sci. **44**, 1509–1524 (1987).
15. W. Möbius, "Zur Theorie des Regenbogens und ihrer experimentellen Prüfung," Abh. Kgl. Sächs. Ges. Wiss. Math.-Phys. Kl. **30**, 105–254 (1907–1909).
16. W. Möbius, "Zur Theorie des Regenbogens und ihrer experimentellen Prüfung," Ann. Phys. (Leipzig) **33**, 1493–1558 (1910).
17. A. B. Fraser, "Why can the supernumerary bows be seen in a rain shower?" J. Opt. Soc. Am. **73**, 1626–1628 (1983) [color plate 1].
18. G. P. Können, "Appearance of supernumeraries of the secondary rainbow in rain showers," J. Opt. Soc. Am. A **4**, 810–816 (1987).
19. J. A. Kneisly, "Local curvature of wavefronts in an optical system," J. Opt. Soc. Am. **54**, 229–235 (1964).
20. J. A. Lock, "Ray scattering by an arbitrarily oriented spheroid. II. Transmission and cross-polarization effects," Appl. Opt. **35**, 515–531 (1996).
21. K. F. Ren, F. Onofri, C. Roze, and T. Girasole, "Vectorial complex ray model and application to two-dimensional scattering of a plane wave by a spheroidal particle," Opt. Lett. **36**, 370–372 (2011).
22. M. V. Berry, "Waves and Thom's theorem," Adv. Phys. **25**, 1–26 (1976).
23. M. V. Berry and C. Upstill, "Catastrophe optics: morphologies of caustics and their diffraction patterns," Prog. Opt. **18**, 257–346 (1980).
24. P. L. Marston and E. H. Trinh, "Hyperbolic umbilic diffraction catastrophe and rainbow scattering from spheroidal drops," Nature **312**, 529–531 (1984).
25. J. F. Nye, "Rainbow scattering from spheroidal drops—an explanation of the hyperbolic umbilic foci," Nature **312**, 531–532 (1984).
26. J. F. Nye, "Rainbows from ellipsoidal drops," Proc. R. Soc. London A **438**, 397–417 (1992).
27. J. A. Lock and F. Xu, "Optical caustics observed in light scattered by an oblate spheroid," Appl. Opt. **49**, 1288–1304 (2010).
28. H. Yu, J. Shen, and C. Tropea, "Application of vector ray tracing to the computation of Möbius shifts for the primary and secondary rainbows," Appl. Opt. **54**, 9093–9101 (2015).
29. F. Xu, J. A. Lock, and C. Tropea, "Debye series for light scattering by a spheroid," J. Opt. Soc. Am. A **27**, 671–686 (2010).
30. J. A. Lock, "Airy theory and the Möbius shift extended to rainbows of all orders," presented at the 10th International Conference on Light and Color in Nature, St. Mary's City, Maryland, USA, 16–20 June 2010.
31. W. J. Glantschnig and S.-H. Chen, "Light scattering from water droplets in the geometrical optics approximation," Appl. Opt. **20**, 2499–2509 (1981).
32. A. Ungut, G. Gréhan, and G. Gouesbet, "Comparisons between geometrical optics and Lorenz–Mie theory," Appl. Opt. **20**, 2911–2918 (1981).
33. R. T. Wang and H. C. van de Hulst, "Rainbows: Mie computations and the Airy approximation," Appl. Opt. **30**, 106–117 (1991).
34. C. L. Adler, J. A. Lock, and B. R. Stone, "Rainbow scattering by a cylinder with a nearly elliptical cross section," Appl. Opt. **37**, 1540–1550 (1998).
35. A. Haußmann, "Observation, analysis, and reconstruction of a twinned rainbow," Appl. Opt. **54**, B117–B127 (2015).
36. A. Haußmann, "Polarized-resolved simulations of multiple-order rainbows using realistic droplet sizes," J. Quant. Spectrosc. Radiat. Transfer **175**, 76–89 (2016).
37. G. P. Können and J. A. Lock, "Rainbows by elliptically deformed drops. II. The appearance of supernumeraries of high-order rainbows," Appl. Opt. **56**, G98–G103 (2017).
38. G. Arfken, *Mathematical Methods for Physicists*, 3rd ed. (Academic, 1985), p. 738, Eq. (13.3.10).
39. A. B. Fraser confirmed that his numerical results of the Möbius shift for the first-order rainbow [17] were based on ray-tracing experiments, not on the Möbius formula (personal communication to G. P. Können, 2016).
40. F. E. Volz, "Der Regenbogen," in *Handbuch der Geophysik VIII*, F. Linke and F. Müller, eds. (Bornträger, 1961), pp. 977–982.
41. G. B. Venturi, *Commentari sopra la storia e la teorie dell'Ottica* (Pe' Fratelly Masi, 1814).
42. H. W. Brandes, "Venturi's Theorie des farbigen Bogens, welcher sich oft an der innern Seite des Regenboges zeigt, dargestellt mit einigen Anmerkungen," Ann. Phys. (Gilbert) **52**, 385–397 (1816).